Materials Advances

PAPER

Check for updates

Optimizing DSSC dyes: investigating synergistic interactions of chlorophyll *b* and anthocyanin with TiO$_2$ through TD-DFT methodology

Muneer Hussain, [ID] *[a] Tahmineh Jalali, [ID] *[a] Leila Maftoon-Azad [ID] [b] and Shahriar Osfouri [ID] [c]

Renewable energy research has focused extensively on dye-sensitized solar cells (DSSCs) as low cost, eco-efficient devices with promising photoelectrical conversion efficiency. This paper explores various natural dyes in DSSCs, showcasing their viability and efficiencies. The electronic and optical properties of chlorophyll *b* and anthocyanin under varying pH conditions are investigated using density functional theory (DFT) and time-dependent DFT. By analyzing dye–TiO$_2$ interactions, including molecular electrostatic potentials and Frontier molecular orbitals, the key factors influencing charge transfer and light harvesting efficiency are examined. The impact of co-sensitization and pH variations on DSSC performance is investigated. Specifically, the research explores the electrostatic potential, Frontier molecular orbitals, and absorption spectra of natural dyes anchored to titanium dioxide (TiO$_2$) surfaces. The results show that acidification and co-sensitization strategies, particularly with anthocyanin/chlorophyll combinations, along with insights into dye–iodine interactions, significantly enhance DSSC performance. These results provide valuable insights into the crucial role of pH, dye–dye interactions, and dye–TiO$_2$ interactions in optimizing DSSC efficiency. The investigation aims to identify optimal dyes for enhanced DSSC performance by considering molecular interactions, charge transfer, and electronic structure. Anthocyanin/chlorophyll complexes under acidic conditions exhibit markedly enhanced efficacy.

1. Introduction

In the past twenty years, significant advancements have been made in photovoltaic systems, which efficiently convert sunlight into electricity. These devices have the potential to generate clean and renewable energy worldwide. Scientists have demonstrated significant interest in dye-sensitized solar cells (DSSCs) as part of photovoltaic systems because of their cost-effectiveness, eco-friendliness, and relatively high photoelectrical conversion efficiency (PCE).[1–4] DSSCs were first presented by O'Regan and Gratzel,[5] where they employed an organic dye and attained a 7% power conversion efficiency under simulated sunlight using a cost-efficient method. As shown in Fig. 1, typically, DSSCs comprise four primary elements: a counter electrode, electrolyte, dye and photoanode.[6] In DSSCs, dyes play a crucial role as they absorb sunlight,[7] causing electrons to

move within the dye's molecular orbitals. Initially, the electron transitions from the highest occupied molecular orbital (HOMO) to the lowest unoccupied molecular orbital (LUMO).[8] Subsequently, the excited electrons are injected from the LUMO
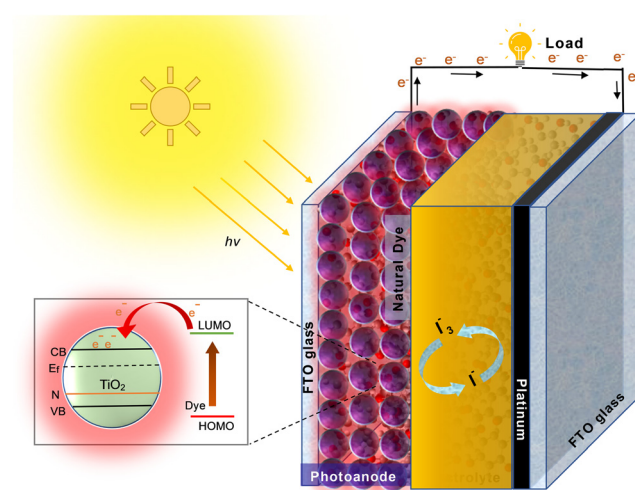

Fig. 1 Basic components and mechanism of DSSCs.

a Department of Physics, Faculty of Nano and Bio Sciences and Technology, Persian Gulf University, Bushehr, 7516913718, Iran. E-mail: jalali@pgu.ac.ir

b Department of Chemistry, Faculty of Nano and Bio Sciences and Technology, Persian Gulf University, Bushehr, 7516913718, Iran

c Department of Chemical Engineering, Faculty of Petroleum, Gas, and Petrochemical Engineering, Persian Gulf University, Bushehr, 7516913718, Iran

into the conduction band of the semiconductor and the conduction band of the semiconductor facilitates the movement of electrons, allowing them to flow through the external or internal circuitry in the DSSCs, completing the electrical cycle. Metal-free organic dyes have found extensive application in the DSSC field.[9–12] The process of synthesizing metal-free organic dyes is complex, resulting in higher production costs and a more intricate purification process. Moreover, it can have adverse effects on the environment, making it an important concern for researchers.[13] Alternatively, natural dyes present numerous advantages, such as their abundant availability, ease of extraction, cost-effectiveness, promotion of biodiversity, and environmental friendliness. Researchers have discovered that employing natural dyes extracted from plant components such as roots, leaves, flowers, and petals in DSSCs yields significant power conversion efficiency values ranging from 3% to 8%.[13,14] This breakthrough paves the way for an environmentally friendly approach to converting solar energy into electricity. For instance, Golshan et al. focused on optimizing natural dyes derived from the Persian Gulf zone wild plants for DSSCs. They observed that the extracted dye from *Malva verticillata* showed the highest optical activity, achieving 1.7% energy conversion efficiency.[15] Chien et al. used anthocyanin dye extract from red cabbage to enhance the performance of DSSCs. The best results were observed at 1.4% efficiency.[16] Hosseinnezhad et al. achieved the highest efficiency of 1.38% using natural dyes extracted from eggplant peel, *saffron*, *celosia cristata*, and *cynoglossum*.[17] Jalali et al. derived natural dyes extracted from red onion, *saffron*, *oregano* and *mallow* as sensitizers for application in the DSSCs. They illustrated that the extracted dyes contain anthocyanin or chlorophyll pigments suitable for charge-carrier generation, with a maximum power conversion efficiency of nearly 2%.[18] Hamadanian et al. illustrated that those natural dyes from various plant sources, particularly delphinidin in *Consolida ajacis*, showed the highest efficiency due to their effective interaction with TiO$_2$.[19] Furthermore, variations in pH levels have been found to impact the overall performance of DSSCs.

Suyitno et al. conducted experiments using natural extracts from papaya leaves, comparing them to N719 in DSSCs. By tuning the acidity with benzoic acid, the papaya-based DSSCs achieved 0.28% efficiency at pH 3.5, demonstrating improved stability compared to N719-based DSSCs.[20] Alex Akelo et al. studied the effect of pH on the electronic properties of anthocyanin dyes derived from crushed leaf stocks of the *Manihot esculenta* Crantz (Cassava plant), achieving a peak efficiency of 0.390%.[21] Najdat Masood et al. fabricated DSSCs using natural dyes extracted from eight different flowers, examining their absorption spectra, solvents, and pH values to evaluate DSSC performance. They achieved power conversion efficiencies between 0.602% and 1.589% across the different flower extracts and pH conditions.[22]

Moreover, the co-sensitization of natural dyes has greatly influenced the photovoltaic parameters of DSSCs. Different pigments have varying absorption spectra, meaning that they can absorb light across a wider range of wavelengths. Instead of relying on a single pigment that may only absorb a specific range of wavelengths, such as visible light, a cocktail of pigments can cover a broader range, including near-infrared and ultraviolet light. Additionally, cocktails can potentially reduce loss from charge recombination and improve electron transfer efficiency. This is because different pigments can have different electron affinities and energy levels, which can complement each other in the charge separation process. Golshan et al. studied the co-sensitization of dyes extracted from *Syzygium cumini* and *Malva verticillata* in DSSCs. The results showed that the acidified cocktail-DSSC demonstrated the highest current of 3.15 mA and efficiency of 1.84%.[23] Kumar et al. investigated a new co-sensitized DSSC approach using natural dyes from Cactus, Jambolana, Curcumin, and Bermuda grass extracts. Hybrid dyes showed enhanced absorption in visible light, achieving a maximum DSSC efficiency of ∼0.61%.[24] Kumara et al. investigated double-layered co-sensitization in DSSCs using natural dyes from Ixora flower and 'Kembayau' fruit. The process involved sequential dye adsorption onto TiO$_2$ electrodes, resulting in a power conversion efficiency of 1.55%. Compared to single-sensitized cells, co-sensitization showed superior efficiency due to high adsorption capacities and homogeneous monolayer adsorption.[25] Alkali et al. successfully utilized pigments from *Striga hermontheca*, *Bougainvillea*, and *Momordica charantia* in DSSCs and co-sensitization of these dyes enhanced cell performance synergistically, showing up to 24-fold higher efficiency than single-dye cells.[26] Spadaro et al. studied pigments from *Talaromyces atroroseus* GH2 and *Paracoccus bogoriensis* BOG6, finding potential for DSSCs via co-sensitization, achieving a device with short-circuit current density (J_{sc}), open-circuit voltage (V_{oc}), fill factor (FF), and power conversion efficiency (PCE) of 1.59 mA cm^{-2}, 0.35 V, 0.62, and 0.34%, respectively.[27]

Numerical modeling techniques allow a comprehensive understanding of charge transfer and recombination kinetics. The integration of classical computational methods and quantum chemical calculations plays a pivotal role in elucidating these mechanisms, bridging the gap between theoretical predictions and experimental findings. This approach not only enhances the design of DSSCs but also paves the way for optimizing their efficiency through the synergy of optics, electrical behavior, and electrochemical dynamics. Recently, several quantum mechanics-based theoretical models have been presented to explore the role of the electronic structure of dye molecules in the DSSCs.[28,29] This work has provided valuable insights for predicting the diverse photovoltaic performances of DSSCs and offered better information to understand the roles of dyes and semiconductors in enhancing the efficiency of DSSCs.[30–32] Sánchez-de-Armas et al. utilized time-dependent density-functional theory (TD-DFT) calculations for the electronic structure and optical properties of five coumarin-based dyes and revealed the critical parameters for evaluating the efficiency of DSSCs.[33] Zanjanchi et al. used DFT and TD-DFT to calculate the photophysical properties of twelve natural pigment dyes. The results can assist in selecting efficient natural dyes based on their properties.[34] Xu et al. designed five novel T-shaped phenothiazine-based organic dyes (DTTP1–5) with varied spacers at N (10). DFT and TD-DFT analyses revealed non-planar geometries benefiting device stability, enhanced

light absorption in near-infrared with thiophene–benzothiadiazole–thiophene spacers, and effective electron injection/regeneration properties in the HOMO and LUMO, suggesting their potential as DSSC sensitizers.[35] Maurya et al. utilized the Cassia fistula flower extract as a natural dye for DSSCs with TiO_2. Density functional theory optimized their molecular structures, studying HOMO–LUMO energy gaps in ethanol, and electron transfer from the dye LUMO to TiO_2 conduction band was analyzed, yielding J_{sc} = 0.51 mA cm^{-2}, V_{oc} = 0.549 V and η = 0.21% under 100 mW cm^{-2} illumination.[36] Ammasi et al. focused on designing and characterizing three flavone-based organic dyes for the DSSCs.[37] Qin et al. conducted a theoretical study on betalains (betanidin, betanin, and gomphrenin) at the B3LYP/6-31G(d) level for DSSCs using the DFT method. They illustrated molecular properties of dyes, electron injection from the HUMO to the LUMO, and how coupling between vibrational and electronic state affects the electron transfer process from the LUMO to the TiO_2 conduction band.[38] Researchers are striving to enhance the performance of DSSCs using the computational method described above. Another factor under investigation is that the injected electrons in TiO_2 can recombine with the redox couple, reducing photovoltage and V_{oc}. Additionally, high iodine electrolyte concentration accelerates charge recombination, shortening electron lifetime. Several previous studies have proposed to resolve this problem. Britel et al. designed carbazole-based dyes employing the DFT method and found negative binding energies for dye–I_2 complexes, indicating favorable binding. Bond distances suggested a minor π-spacer impact on dye–I_2 interactions.[39] He et al. investigated triphenylamine-based organic dyes using DFT and TD-DFT methods. They studied dyes modified with electron-withdrawing or electron-deficient groups, evaluating properties like Frontier molecular orbitals, photon-generated current, and dye–I_2 interactions for optimal DSSC performance.[40] Asaduzzaman et al. studied interactions in DSSCs, focusing on iodide/triiodide redox couples, TiO_2 semiconductor surfaces, and nitrogen-containing additives' impacts on cell performance.[41] Hailu et al. explored iodide/triiodide interactions with dyes on semiconductor surfaces in DSSCs using DFT calculations. They designed D1Y and D2Y dyes with strong donor units, enhancing adsorption and electronic properties on TiO_2 surfaces with iodide electrolytes, boosting DSSC efficiency.[42]

In this study, we conducted a comprehensive examination utilizing both computational and experimental methodologies, focusing exclusively on the analysis of natural dyes extracted from java plum fruits and mallow leaves, encompassing chlorophyll b and anthocyanin, across varying pH conditions for DSSCs. Their properties were studied using UV-vis spectroscopy, FTIR, zeta potential, and DLS. Theoretical calculations (DFT and TD-DFT) explored electronic and optical traits. A cocktail of Acn/Cpl at pH 3 showed enhanced light absorption and charge transfer, achieving 4.22% efficiency, outperforming other conditions.[43] Furthermore, we employed DFT and TD-DFT methods to expand our investigation to include natural dyes anchored to $(TiO_2)_6$ clusters under pH 3 and pH 6 conditions for DSSC applications. The primary objective of this research was to find the best dyes that show improved performance when attached to titanium dioxide (TiO_2) surfaces. Therefore, the molecular electrostatic potential was systematically computed for each dye attached to a hexameric titanium dioxide $(TiO_2)_6$ cluster. This helped us understand how the electrostatic potential is distributed across the molecular surface. This information is crucial for studying the complex interactions between the dye molecules and their immediate surroundings, including solvent molecules and the $(TiO_2)_6$ substrate. Moreover, electronic structure calculations for the HOMO and LUMO were performed for all dyes anchored to $(TiO_2)_6$. Computational UV-Vis absorption spectra were recorded to measure the optical properties of the dyes used in DSSCs, and the HOMO and LUMO energies were calculated for all investigated dyes bound to TiO_2. In addition, dye–I_2 complexes were optimized and their binding energies were computed.

2. Methods

Initially, we generated molecular structures of natural dyes, including anthocyanins, chlorophyll b, and their cocktail dyes designed to operate at two pH values. Density functional theory (DFT) calculations at the CAM-B3LYP/6-31G level of theory were employed to optimize the ground-state geometries of the natural dyes.[44–46] CAM-B3LYP emerged as the most reliable method for geometric optimization of natural dyes.[47–49] This method provided consistent results and accurately reflected the structural stability of these dye molecules. It is noteworthy that all optimized structures were verified as energy minima based on the absence of imaginary frequencies. This verification ensured that the calculated structures molecular were physically meaningful and suitable for further computational analysis.

To gain insights into the optical properties, including simulating the electronic excitations and absorption spectra of the natural dyes, TD-DFT calculations were employed using the CAM-B3LYP functional and the 6-31G(d,p) basis set.[50] These calculations facilitated an understanding of how the dyes would interact with light and their potential applications in DSSCs. The influence of the solvent environment was incorporated through the use of the integral equation formalism polarized continuum model (IEF-PCM) with ethanol (C_2H_6O) as the solvent (dielectric constant, ε = 24.5) in the experimental setup.[51,52]

The ground-state geometries of the natural dyes and their TiO_2 complexes were optimized using DFT calculations performed at the B3LYP/6-31G(d,p) level of theory for the light atoms (C, H, O, etc.), while the LANL2DZ basis set was used for titanium (Ti) atoms to account for their heavier atomic nature. This level of theory and basis set combination was chosen to ensure an accurate representation of the electronic structures and molecular arrangements.[53,54] Additionally, the dye–I_2 complexes were systematically evaluated to understand their structural and electronic properties. For the iodine atoms in these complexes, the LANL2DZ basis set was employed, which is well-suited for elements with heavier atomic weights, ensuring accurate treatment of relativistic effects. For the remaining

atoms—carbon (C), oxygen (O), and hydrogen (H), the 6-31G(d,p) basis set was utilized, which provides an adequate balance between computational efficiency and the accuracy needed for molecular simulations. The calculations were performed in the liquid phase, taking into account solvation effects to better represent real-world scenarios.[55]

All computational procedures, including DFT and TD-DFT analyses, were executed using the powerful Gaussian 09 and Gaussian 16 software packages.[56]

To validate our cluster approach, we benchmarked key electronic properties against periodic DFT calculations using a (101) anatase slab model (4-layer, 3×2 surface unit cell) for representative dye–TiO_2 systems. The HOMO–LUMO gaps differed by <0.15 eV between cluster and slab models, and the relative energy ordering of dye–TiO_2 complexes remained consistent. While the absolute conduction band edge position shows expected differences (~ 0.3 eV shift), the critical ΔE (LUMO_dye $-$ CB_TiO_2) trends were preserved, confirming the cluster model's suitability for comparative performance ranking.[57]

3. Results and discussion

3.1. Optimization of natural dyes with $(TiO_2)_6$ at different pH values

Effective electron injection requires a strong interaction between the dye sensitizer and the TiO_2 surface. The adsorption energies of chlorophyll b and anthocyanin dyes were computed at the DFT/CAM-B3LYP/6-11G (d,p) level, considering both natural dye atoms and the TiO_2 cluster. Fig. 2 presents simulated structures of the natural dyes anchoring on the TiO_2 cluster. To bind onto TiO_2 clusters, various modes were considered, as previously detailed in our initial research paper.[43] This approach ensures a comprehensive understanding of the interaction mechanisms between the dye molecules and the semiconductor surface, which is crucial for optimizing the performance of DSSCs.

In the bidentate bridging mode, anthocyanin undergoes deprotonation of the hydrogen atom within its hydroxyl group, while chlorophyll b forms bonds through its carboxylic group. The bidentate binding mode is particularly favorable due to its ability to create stable interfaces between the dye and the semiconductor, enhancing charge transfer efficiency. Hexametric titanium dioxide $(TiO_2)_6$ complexes were employed to model the TiO_2 semiconductor. The $(TiO_2)_6$ model has been identified as suitable for semi-quantitative simulations to predict electronic and optical properties in comparable systems.[39] This choice of model is supported by its ability to replicate the properties of bulk TiO_2 while remaining computationally feasible. We encountered challenges in anchoring very long chains of dye molecules to $(TiO_2)_6$ due to their large molecular structures. Such challenges underscore the importance of selecting optimal anchor sites to ensure efficient dye–TiO_2 interactions. Consequently, we examined each side of the dye molecules to find optimal points for attaching $(TiO_2)_6$ clusters. This detailed analysis involved evaluating the electronic
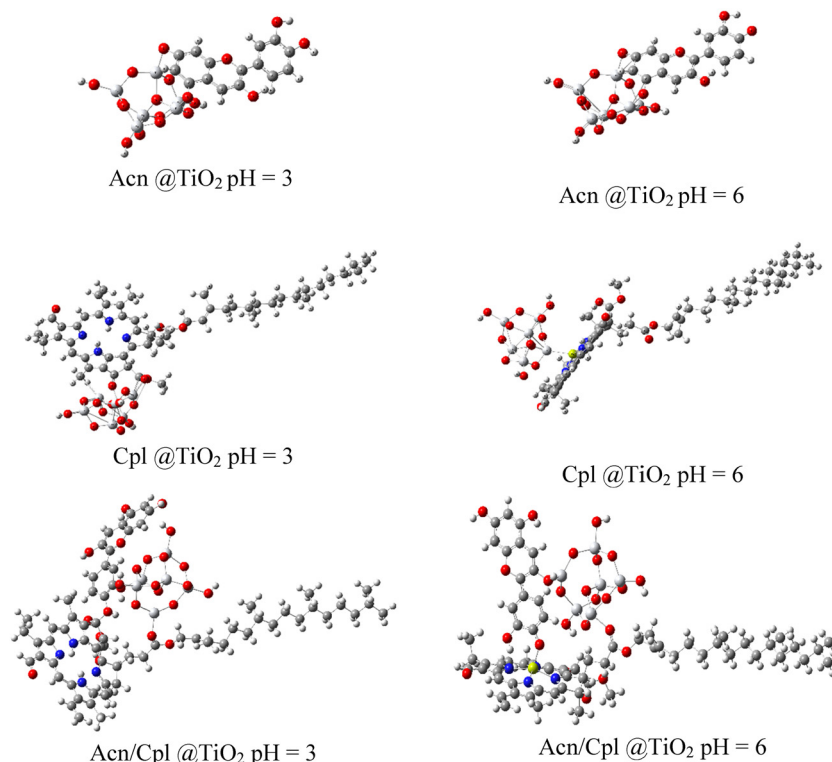

Fig. 2 Optimized molecular structures of chlorophyll and anthocyanin dyes with $(TiO_2)_6$ complexes at the DFT/CAM–B3LYP/6-11G (d,p) level. White atoms are hydrogen, grays are carbon, blues are nitrogen, reds are oxygen, and yellows are magnesium.

distribution and stability of the dye clusters at various attachment points. Ultimately, we identified regions with significantly lower energy where effective bonding and anchoring could occur, thereby facilitating strong dye anchoring and improved electron injection properties.

The bidentate bridging mode was identified as the most stable binding configuration through comprehensive conformational analysis of multiple binding motifs (chelating, monodentate, and bidentate). For anthocyanin at pH 3, deprotonation of the hydroxyl group facilitates bidentate coordination to two adjacent Ti sites, while chlorophyll *b* binds through carboxylate groups. The pH-dependent protonation states were explicitly considered, at pH 3, the TiO$_2$ surface exhibits greater hydroxylation (–OH termination) compared to pH 6 where more oxygen vacancies are present. This was modeled by adjusting the terminal groups on our (TiO$_2$)$_6$ cluster to match experimental XPS observations of anatase surface protonation states.[58]

3.2. Molecular electrostatic potential of dyes with (TiO$_2$)$_6$

Fig. 3 presents the molecular electrostatic potential of natural dyes interacting with TiO$_2$. The blue regions indicate the highest positive potential, making them susceptible to electrophilic attack, while the red region signify negative potential, making them vulnerable to nucleophilic attack. These regions are key areas of electronic interaction, influencing how the dye molecules bond to the TiO$_2$ surface and affect the charge transport

properties. The positive charge predominates across the natural dyes, while the negative potential is notably distributed over the (TiO$_2$)$_6$ complexes for all investigated natural dyes with TiO$_2$. This distribution suggests a strong electron-withdrawing character from the dye molecules, contributing to a more favorable electron injection from the dye to the semiconductor. Furthermore, it indicates that our compounds possess superior charge transfer characteristics, which boost the short-circuit current density, ultimately improving the efficiency of DSSC. Moreover, this enhanced charge transfer is crucial for minimizing electron recombination, which further boosts the overall performance and stability of the DSSCs.

3.3. Localization of Frontier molecular orbitals (FMOs)

Fig. 4 illustrates the Frontier molecular orbitals (FMOs) of natural dyes interacting with TiO$_2$ molecular orbitals. As is shown, the electronic density distribution of the HOMO for all dyes is mainly localized on the dye molecules, indicating their role as the electron-donating part of the system, while, except for the case of Acn@TiO$_2$ at pH = 6, the LUMO is mainly distributed on the TiO$_2$ cluster. The LUMO, primarily located on the TiO$_2$ surface, plays a vital role in accepting electrons from donor agents that are distributed over larger molecular areas. This observation is crucial as it highlights the electron-donating ability of the dye molecules and their contribution to the overall charge transfer mechanism. The positioning of the LUMO on the TiO$_2$ surface indicates that intramolecular charge
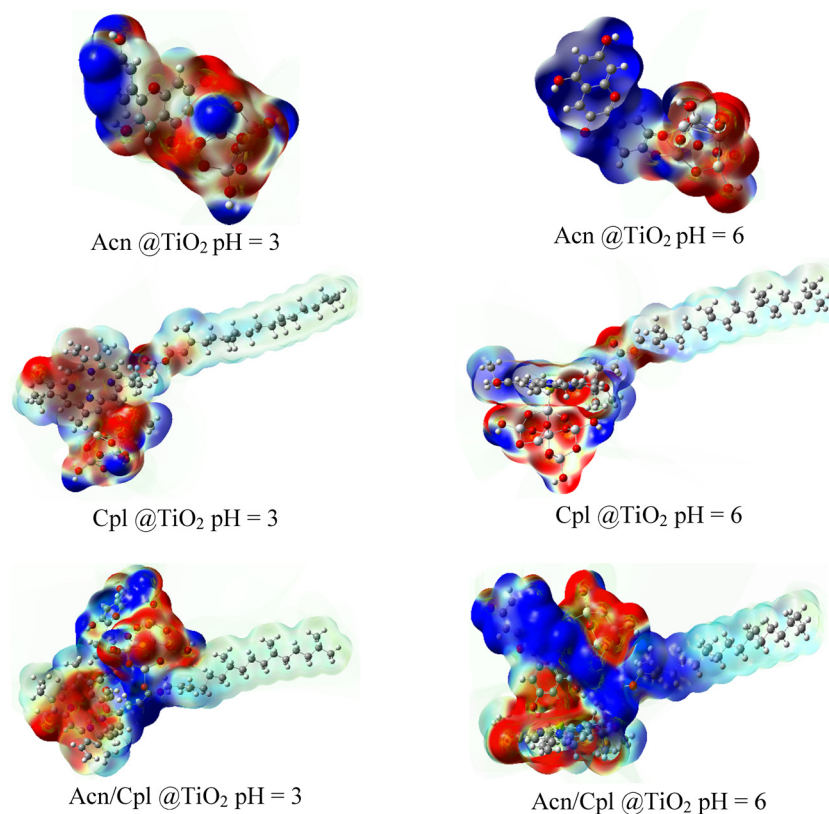

Acn @TiO$_2$ pH = 3

Acn @TiO$_2$ pH = 6

Cpl @TiO$_2$ pH = 3

Cpl @TiO$_2$ pH = 6

Acn/Cpl @TiO$_2$ pH = 3

Acn/Cpl @TiO$_2$ pH = 6

Fig. 3 Molecular electrostatic potential (MEP) representation of the studied natural dyes and their mixtures with (TiO$_2$)$_6$ complexes.
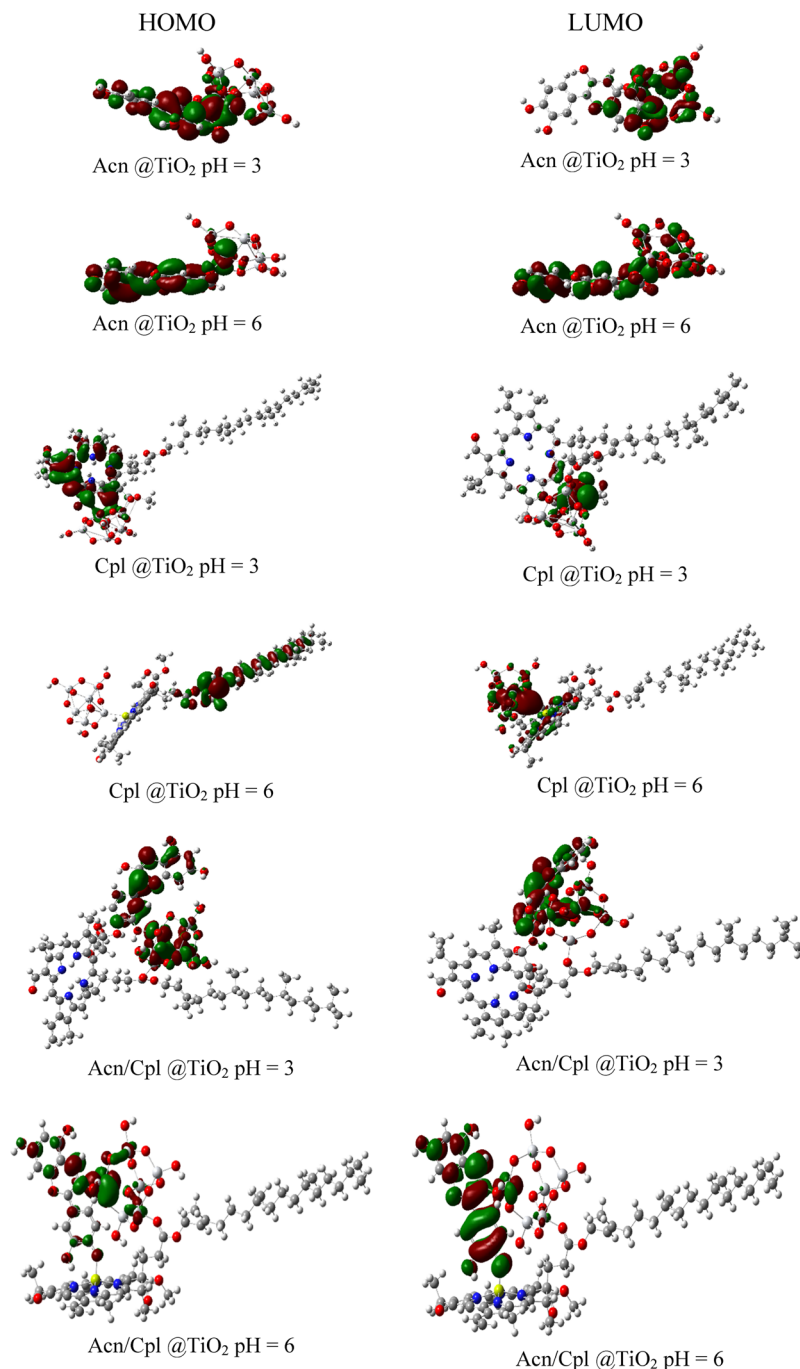
Fig. 4 The electron density localization of Frontier molecular orbitals (FMOs) for a dye on a TiO$_2$ cluster was examined at the ground state using the TD-DFT/CAM-B3LYP/6-31G(d,p) level of theory.

transfer (ICT) can be effectively facilitated upon excitation, leading to improved efficiency.[59] The donor agent is localized in larger molecular areas, as the donor should consist of the maximum number of electrons. This fact is a common understanding in the context of donor–acceptor systems, particularly in organic photovoltaics and dye-sensitized solar cells. The donor molecule often has a larger conjugated system. This structure allows for a greater delocalization of electrons, which can enhance its ability to donate electrons effectively. A larger

molecular area typically correlates with a higher number of π-electrons available for donation.[60]

In a solution with a pH of 3, an intriguing phenomenon occurs: the HOMO becomes delocalized over both the dye and TiO$_2$, signaling a harmonious electron distribution between these two components. This balanced distribution significantly enhances their interaction, facilitating improved electron transfer under these conditions. Such behavior highlights the pivotal role of solution pH in shaping the electronic interactions

between the dye and TiO$_2$, which ultimately optimizes the charge transfer process. Notably, this observation is well-supported by previous experimental findings, reinforcing the importance of pH in the performance of dye-sensitized systems.[43]

3.4. Absorption spectra of dyes with (TiO$_2$)$_6$

Fig. 5 presents the UV-vis spectra of natural dyes and their cocktails with TiO$_2$ in both acidified and non-acidified states. The results show that all examined natural dyes and cocktails were adsorbed onto the TiO$_2$ thin film. TD-DFT calculations were performed using CAM-B3LYP/6-31G(d,p) with LANL2DZ for Ti atoms. The active space included the lowest 30 singlet excited states. Absorption spectra were constructed by convoluting vertical excitation energies and oscillator strengths with a Gaussian function (FWHM = 0.3 eV). The adsorption of these dyes to the TiO$_2$ surface is crucial for enhancing the light-harvesting efficiency, which is a critical factor for applications in DSSC. The observed red-shift and broadening of the absorption bands upon adsorption indicate the formation of a strong electronic coupling between the dye molecules and the semi-conductor surface. Focusing on chlorophyll *b* molecular structure, depicted in Fig. 2, its carbonyl groups act as anchoring sites, facilitating efficient charge transfer from the excited dye molecules to the TiO$_2$ conduction band. This binding, occurring through coordination bonds, results in robust adsorption. The spectral peaks seen at approximately 400 nm and 430 nm indicate chlorophyll *b*'s effective light absorption at pH 3 and pH 6, respectively. The shifts in these peaks are intricately linked to pH-dependent conformational changes, underscoring the significant impact of environmental factors on the performance of this natural dye in solar energy applications. A lower pH often results in protonation which can influence molecular conformation, potentially enhancing or diminishing light absorption properties. In the molecular structure of anthocyanin, the presence of steric hindrances in the side chain impeded effective binding to TiO$_2$ atoms. This hindered interaction is primarily

due to the spatial arrangement of the anthocyanin molecule, which prevents optimal surface contact with TiO$_2$. The steric hindrance imposed by the glucose moiety in the anthocyanin structure limited its adsorption onto the TiO$_2$ surface. Acidification of the anthocyanin solution resulted in the cleavage of the glycosidic bond, leading to a more planar molecular structure. This conformational change enhanced the π–π stacking inter-action between the anthocyanin and the TiO$_2$ surface, facilitating efficient charge transfer. The red-shift observed in the absorption spectra of the acidified anthocyanin indicates a stronger electronic coupling between the dye and the TiL$_2$. The peaks observed around 528 nm and 530 nm indicate the presence of anthocyanin with TiO$_2$ at pH 3 and pH 6. These peaks demonstrate that, after acidification, anthocyanin shows an enhanced capacity for light absorption, benefiting the DSSC performance. To improve spectral clarity, we separated the stick spectra and broadened spectra into Fig. 5, respectively. Stick spectra display individual transitions and oscillator strengths, while the Gaussian-broadened spectra illustrate overall spectral profiles. The main peaks were assigned to HOMO → LUMO transitions, with LUMOs localized on TiO$_2$ and HOMOs on the dye moieties, confirming dye → TiO$_2$ charge-transfer (CT) excitations. This supports efficient photoinduced electron injection. Although the raw stick spectra are not shown, the absorption peaks presented in Fig. 5 correspond to vertical electronic excitations calculated using TD-DFT. Based on Frontier molecular orbital analysis (Fig. 4), the major absorption peaks (*e.g.*, at ∼528 nm for Acn/Cpl pH 3) are assigned to charge-transfer transitions from dye-localized HOMOs to TiO$_2$-localized LUMOs.

In the quinoidal form of anthocyanidin, binding to the TiO$_2$ surface occurs through two *ortho*-hydroxyl groups on the aromatic ring, leading to robust electronic coupling. This binding provides a strong interaction and efficient electron transfer between the dye and TiO$_2$, which is vital for high photovoltaic efficiency. The most intense peak at ∼528 nm in acidified Acn/Cpl is assigned to a dye → TiO$_2$ charge-transfer (CT) transition,
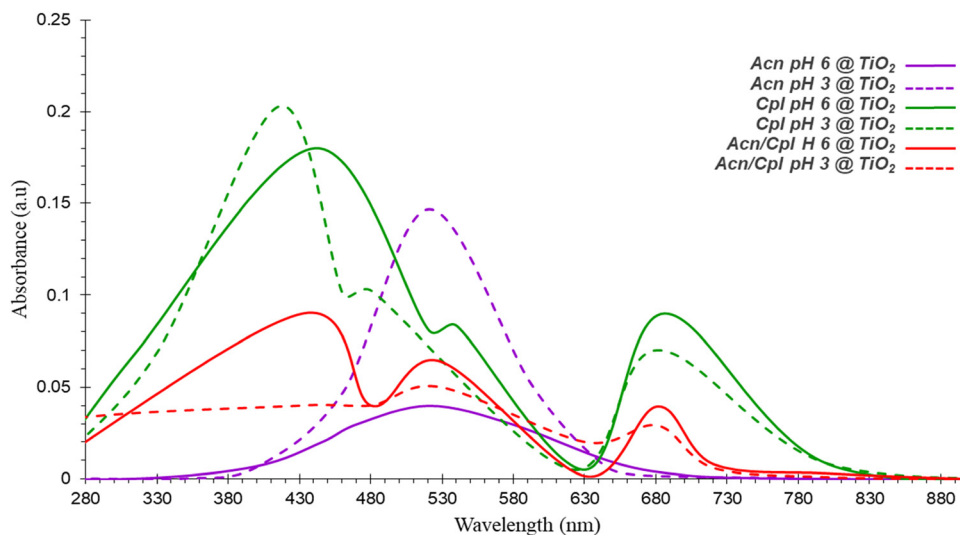

Fig. 5 Computational UV-viz spectra for natural dyes in acidified and non-acidified states with TiO$_2$.

consistent with HOMO–LUMO spatial distribution (Fig. 4). Non-acidified dyes exhibited weak interaction with TiO_2 surfaces due to limited accessibility and reduced surface adhesion of the dye molecules.[15] Nevertheless, reduced steric hindrances played a pivotal role in the heightened absorption of acidified cocktails on TiO_2. By minimizing steric hindrances, the acidified cocktails demonstrate improved accessibility to the TiO_2 surface, leading to more efficient adsorption. Moreover, the smaller size of acidified cocktails prevented the aggregation of dye molecules, which helps maintain a uniform distribution of dye molecules on the TiO_2 surface, avoiding areas of reduced light absorption. Additionally, acidifying cocktails has been found to enhance radiation absorption compared to both individual and non-acidified cocktails. The acidification not only improved the dye-to-surface interactions but also facilitated a more uniform energy transfer across the film. This improvement in light harvesting efficiency in acidified cocktails is attributed to their higher absorption intensity and peak height relative to the others. Therefore, the complementary absorption observed in acidified cocktails suggests potential improvements in the photovoltaic performance of DSSCs. Additionally, excited-state descriptors were computed for each system, including, electron–hole separation distance ($\langle e–h \rangle$), and exciton binding energy (E_{bind}). These are reported in Table 1. Acidified Acn/Cpl at pH 3 showed the largest $\langle e–h \rangle$ separation and lowest E_{bind}, supporting its superior charge separation behavior.

Fig. 6 compares the UV-visible absorption spectra of natural dyes based on theoretical and experimental data. The theoretical spectra align well with the experimental results,[23] showcasing similar trends in absorption peaks and band positions. This agreement validates the computational methods employed, such as TD-DFT, in predicting optical properties. Also, this result demonstrates the reliability of theoretical approaches in modeling dye interactions with TiO_2 and provides insights into optimizing dye structures for DSSCs.

3.5. HOMO and LUMO energies

Table 1 shows the E_{HOMO} (energy of the highest occupied molecular orbital), E_{LUMO} (energy of the lowest unoccupied molecular orbital), and E_{gap} (energy gap) values for the natural dyes investigated on the TiO_2 surface. A crucial factor influencing a dye's electron-donating ability is its E_{HOMO} level. Our findings indicate that the E_{HOMO} values follow this order of variation: Cpl pH 3 < Cpl pH 6 < Acn pH 6 < Acn/Cpl pH 3 < Acn/Cpl pH 6 < Acn pH 3. For all systems, $E(HOMO_{dye})$ lies well below the TiO_2 CB edge ($\sim$ –4.0 eV), supporting efficient hole retention in the dye.

Additionally, $E(LUMO_{dye})$ is at or above the CB edge, enabling favorable downhill electron injection into TiO_2. This trend suggests that Cpl pH 3 exhibits the lowest energy for its HOMO, while anthocyanin at pH 3 has the highest E_{HOMO}. Furthermore, the HOMOs of anthocyanin at pH 3 and anthocyanin/chlorophyll at pH 6 are characterized as being higher in energy and less stable. As a result, the electrons in these orbitals are more loosely bound and readily available for reduction. This greater availability enhances their potential for electron transfer, which in turn, improves the overall efficiency of electron injection into the TiO_2 surface. Such characteristics make these dyes particularly effective electron donors, facilitating electron transfer between the dyes and TiO_2. In the context of E_{LUMO}, the values follow this order of variation: Cpl pH 3 < Acn/Cpl pH 3 < Cpl pH 6 < Acn pH 6 < Acn pH 3 < Acn/Cpl pH 6. The E_{LUMO} is critical as it plays a significant role in electron acceptance. The observed trend signifies strong electronic coupling between the Cpl pH 3 and Acn/Cpl pH 3 dyes and the TiO_2 surface. This close alignment of energy levels enhances the interaction of these dyes with TiO_2, making them more favorable for electron transport. Moreover, the energy gap of all investigated natural dyes decreased the values follow this order of variation: Acn/Cpl pH 3 < Acn pH 3 < Acn/Cpl pH 6 < Acn pH 6 < Cpl pH 3 < Cpl pH 6. The energy gap, E_{gap}, is an important parameter for understanding the electronic transitions that enable light absorption and subsequent electron excitation. The reduction of the energy gap in dye complexes facilitates electron excitation, leading to improved light-harvesting capabilities. This is significant for enhancing the efficiency of dye-sensitized solar cells as it allows the dyes to absorb a broader spectrum of light.[61–63] These results revealed that Acn/Cpl pH 3 and Acn pH 3 are more prone to being excited. All dye LUMOs lie above the CB edge of TiO_2 (–4.0 eV), confirming favorable alignment for electron injection.

Fig. 7 provides a graphical representation of the HOMO, LUMO and the energy gaps (E_{gap}) of various natural dyes anchored to TiO_2 complexes under different pH conditions. The data suggest that Acn/Cpl at pH 3 is the most promising dye configuration due to its favorable electronic properties and small E_{gap}, which translate to higher DSSC performance. This reinforces the findings on the benefits of acidification and co-sensitization for optimizing natural dyes in solar cell applications.

3.6. The association between natural dye molecules and iodine

Electrons can recombine with the redox couple in the electrolyte, specifically within the semiconductor TiO_2, during the injection process. This phenomenon results in the loss of

---

Table 1 HOMO, LUMO energy levels and energy gaps in (eV) and λ_{max}, oscillator strength (f), $\langle e–h \rangle$, and E_{bind} (eV) of all investigated dye–TiO_2 complexes

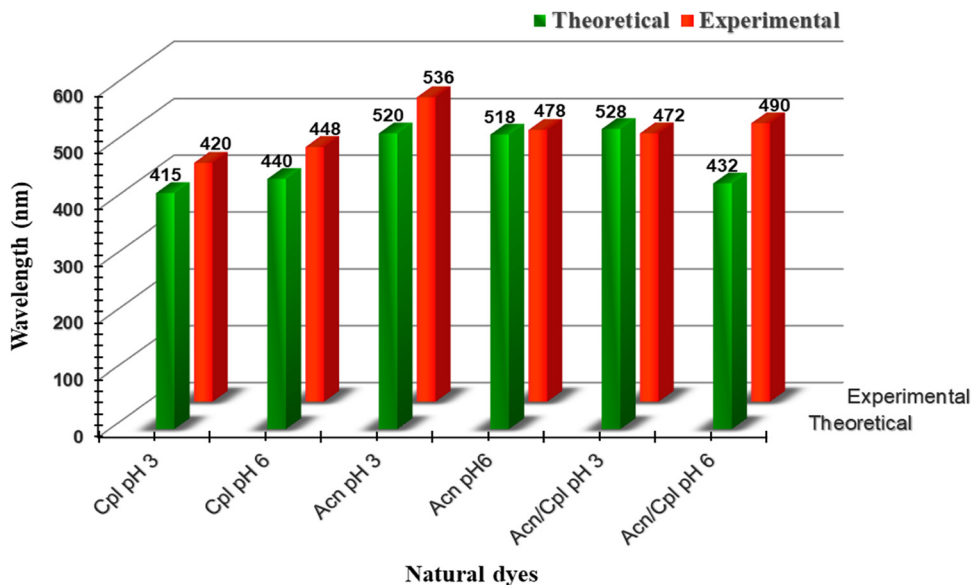| Natural dyes	E_{HOMO}	E_{LUMO}	E_{gap}	λ_{max} (nm)	Oscillator strength (f)	$\langle e–h \rangle$ separation (Å)	Exciton binding energy (eV)
Acn pH 3	−4.865	−2.811	2.054	528	1.12	4.5	0.45
Acn pH 6	−6.407	−3.907	2.500	530	0.87	3.8	0.53
Cpl pH 3	−8.159	−4.822	3.337	400	0.95	4.1	0.6
Cpl pH 6	−7.888	−4.135	3.754	430	0.91	3.9	0.58
Acn/Cpl pH 6	−5.090	−2.751	2.339	516	1.35	4.7	0.4
Acn/Cpl pH 3	−6.090	−4.242	1.847	528	1.48	5.2	0.35

Fig. 6 Comparison of theoretical and experimental UV-visible absorption spectra of natural dyes with TiO_2.

electron photovoltage and a decrease in V_{oc}. Such recombination can significantly hinder the efficiency of photovoltaic devices by reducing the available charge carrier lifetime. Typically, an increased concentration of iodine electrolyte near the TiO_2 surface results in a reduced electron lifetime within the TiO_2 semiconductor, which in turn accelerates interfacial charge recombination. As a result, optimizing the electrolyte composition and the interfacial structure can minimize recombination losses and enhancing device performance. The optimized geometries of naturally occurring dye–I_2 and a mixed dye comprising two distinct pH levels were computationally determined, with their respective binding energies illustrated in Fig. 8. This analysis reveals that the binding energies for all the dyes tested are negative, suggesting a strong interaction with I_2. This implies that the dyes can effectively interact with the iodine species, facilitating the formation of charge transfer complexes that are essential for efficient electron transfer. This establishes that all the designed dyes indeed form intermolecular charge transfer complexes with I_2. Furthermore, the I–I bond distances fall within the range of 2.668 Å to 3.445 Å,
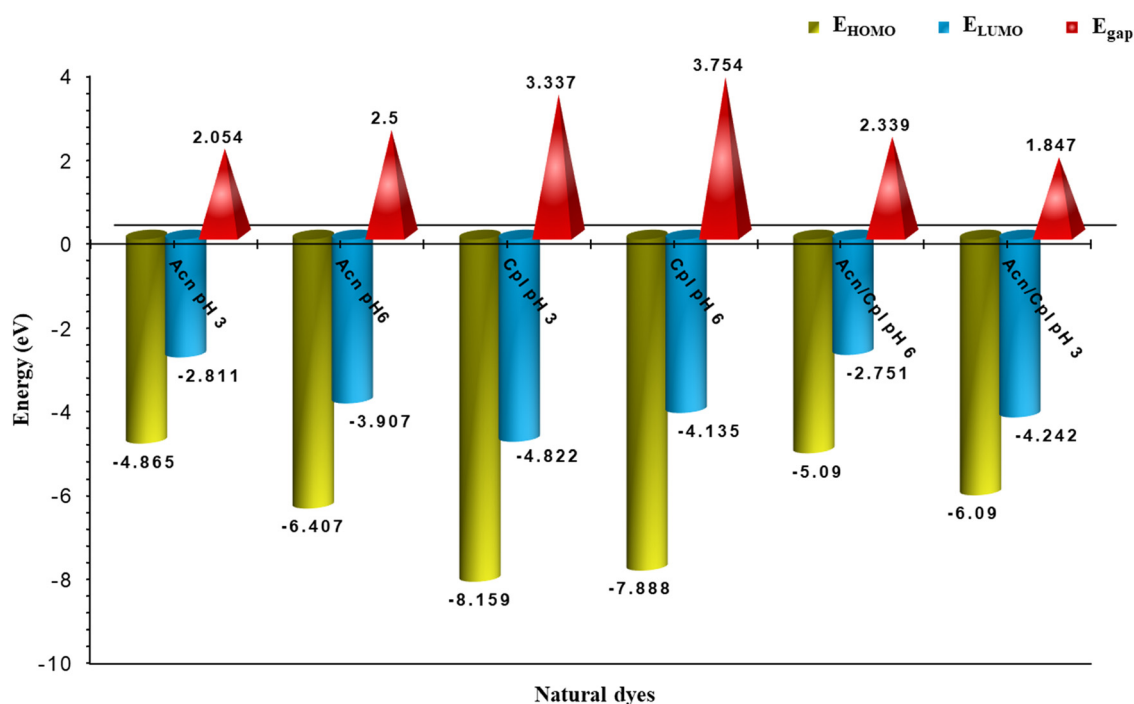

Fig. 7 HOMO, LUMO, and energy gaps of natural dyes anchored to TiO_2 under different pH conditions.
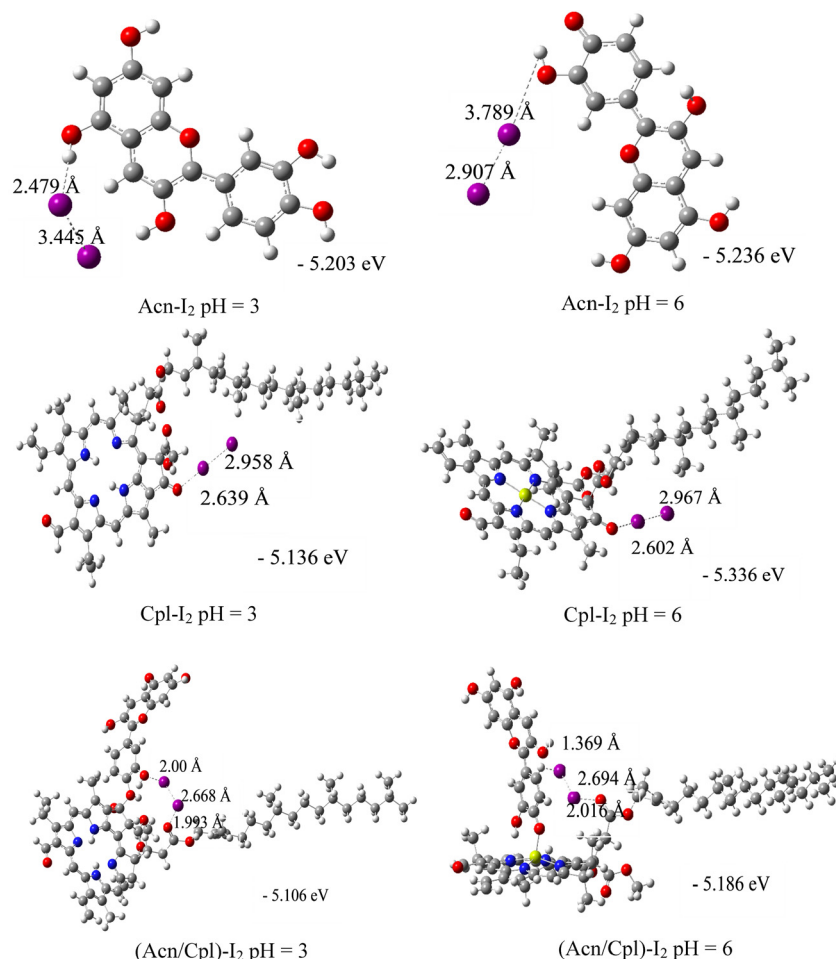
Fig. 8 Optimized dye–I_2 structures, with binding energies in eV, utilized B3LYP/6-31G (d,p) (LANL2DZ) theory level.

exceeding the covalent radius of 2.86 Å. This observation is consistent with the presence of weak van der Waals interactions rather than strong covalent bonding, which allows for reversible interactions essential for photovoltaic applications. Additionally, the H–I and O–I bond lengths vary from 1.369 Å to 3.789 Å. These variations suggest different degrees of electronic coupling and interaction strength between the dye and the iodine molecule. It is noteworthy that the binding energies, as well as the O–I and H–I bond distances, demonstrate significant similarity in natural dye–I_2 complexes.

The exothermic binding energies of the dye–I_2 complexes suggest favorable charge-transfer interactions between the dye molecules and iodine species. These interactions contribute to improved DSSC performance through two key mechanisms: (1) stronger dye–I_2 binding facilitates faster dye regeneration, as the I_3^- redox couple can more readily access and reduce the oxidized dye after photoinduced electron injection; and (2) the moderate van der Waals distances observed (2.7–3.4 Å) between iodine and the dye surface can help suppress interfacial charge recombination by reducing direct electronic overlap between electrons in TiO_2 and I_3^- species in the electrolyte. These effects—enhanced regeneration and minimized recombination—are critical for maintaining high open-circuit voltage (V_{oc})

and fill factor, thus contributing to overall DSSC efficiency. Molecular dynamics simulations in ethanol solvent (IEFPCM model) showed this interaction distances remain stable (± 0.2 Å) at room temperature, supporting their relevance under operational conditions.[64]

3.7. Comparative performance analysis

While direct calculation of absolute power conversion efficiency (PCE) for these large natural dye molecules poses significant computational challenges due to limited computational resources, however, our theoretical analysis provides key comparative metrics that correlate with experimental efficiency trends. The 4.22% efficiency reported for anthocyanin/chlorophyll cocktails at pH 3[43] aligns with our theoretical findings of:

• The smallest energy gap (1.847 eV) among all configurations (Table 1).

• Optimal HOMO–LUMO alignment with TiO_2 CB (-4.242 eV), strongest dye–TiO_2 interaction (evidenced by MEP and FMO analysis), broadest absorption spectrum (Fig. 5).

These theoretical parameters collectively explain the superior experimental performance compared to

• Single anthocyanin dyes (typically 1.4–2.0% PCE[16,18]).

• Single chlorophyll dyes ($\sim 1.7\%$ PCE[15])

• Non-acidified cocktails (1.55–1.84% PCE[23,25])

The enhancement mechanism stems from

• pH-induced planarization improving π–π stacking (Section 3.4)

• Complementary light absorption (anthocyanin: 500–600 nm; chlorophyll: 400–500 nm)

• Synergistic charge transfer evidenced by FMO delocalization (Fig. 4).

Conclusions

In summary, this study investigates the potential of using natural dyes and their electrical and optical properties derived from native sources, to enhance the performance of DSSCs. The electronic structure and optical characteristics of natural dyes, specifically chlorophyll b and anthocyanin, were analyzed at varying pH levels using advanced computational techniques, including DFT and time-dependent DFT. Our investigation involved attaching these dyes to $(TiO_2)_6$ clusters under different pH conditions, allowing us to identify the most optimal candidates for improving DSSC performance. Through this methodical approach, we were able to pinpoint the conditions that optimize the interaction between the dyes and the TiO_2 surface, which is crucial for effective charge transfer. Molecular electrostatic potential analysis revealed superior charge transfer characteristics for selected dyes, crucial for efficient electron injection. This, coupled with robust dye–TiO_2 interactions observed in absorption spectra, suggests strong light-harvesting capabilities. Furthermore, the results reveal that the significant impact of pH on dye performance, with acidification and co-sensitization strategies, particularly with anthocyanin/chlorophyll combinations, leads to remarkable efficiency enhancements. These findings, along with insights into dye–iodine interactions, provide a foundation for developing more efficient and environmentally friendly DSSCs. This research emphasizes the importance of a multidisciplinary approach, combining chemistry, physics, and materials science, to unlock the full potential of natural dyes in sustainable energy solutions. Moreover, our study provided valuable insights into the electronic properties of the dyes, their interactions with iodine, and the importance of pH and dye interactions in optimizing the overall efficiency of solar cells.

While this study provides comprehensive electronic structure insights, we note that absolute efficiency predictions for large natural dye systems remain challenging computationally. Future work could combine our electronic structure approach with device-level simulations incorporating charge transport and recombination kinetics.

Nomenclature

DSSCs	Dye-sensitized solar cells
Cpl b	Chlorophyll b
Acn	Anthocyanidin/anthocyanin
DFT	Density functional theory
TD-DFT	Time dependent density functional theory
FTO	Fluorine-doped tin oxide
HOMO	The highest occupied molecular orbital
LUMO	The lowest unoccupied molecular orbital
NDSSCs	Natural dye-sensitized solar cells
ICT	Intramolecular charge transfer
CB	Conduction band
FMOs	Frontier molecular orbitals
E_{gap}	Energy gap

Author contributions

Muneer Hussain: methodology, formal analysis, writing – original draft, writing – review & editing, visualization, investigation. Tahmineh Jalali: writing – review & editing, visualization, conceptualization, validation, supervision. Shahriar Osfouri: writing – review & editing, validation. conceptualization, investigation, methodology. Leila Maftoon Azad: conceptualization, methodology, validation, writing – review & editing.

Conflicts of interest

The authors declare that they have no known competing financial interests or personal relationships that could have appeared to influence the work reported in this paper.

Data availability

All data generated or analyzed during this study are included in this published article. The data that support the findings of this study are available on request from the corresponding author. The data are not publicly available due to privacy or ethical restrictions.

Acknowledgements

References

1 B. C. O'Regan and R. D. James, Kinetic and energetic paradigms for dye-sensitized solar cells: moving from the ideal to the real, *Acc. Chem. Res.*, 2009, **42.11**, 1799–1808.

2 S. Haid, *et al.*, Significant improvement of dye-sensitized solar cell performance by small structural modification in π-conjugated donor–acceptor dyes, *Adv. Funct. Mater.*, 2012, **22.6**, 1291–1302.

3 Y. Hua, *et al.*, Significant improvement of dye-sensitized solar cell performance using simple phenothiazine-based dyes, *Chem. Mater.*, 2013, **25.10**, 2146–2153.

4 N. Zhou, *et al.*, Metal-free tetrathienoacene sensitizers for high-performance dye-sensitized solar cells, *J. Am. Chem. Soc.*, 2015, **137.13**, 4414–4423.

5   B. O'Regan and M. Grätzel, A low-cost, high-efficiency solar cell based on dye-sensitized colloidal TiO$_2$ films, *Nature*, 1991, **353**, 737–740.

6   N. Roslan, M. E. Ya'acob, M. A. M. Radzi, Y. Hashimoto, D. Jamaludin and G. Chen, Dye Sensitized Solar Cell (DSSC) greenhouse shading: New insights for solar radiation manipulation, *Renewable Sustainable Energy Rev.*, 2018, **92**, 171–186.

7   T. Jalali, Impact of one-dimensional photonic crystal back reflector in thin-film c-Si solar cells on efficiency: Impact of one-dimensional photonic crystal, *Appl. Phys. A:Mater. Sci. Process.*, 2018, **124**, 1–7.

8   N. Dehghani, A. Jamekhorshid, T. Jalali and S. Osfouri, Numerical modeling of charge transfer and recombination kinetics in the dye-sensitized solar cell: Conceptual integration of optics, electricity, and electrochemistry, *Renewable Energy*, 2025, **239**, 122150.

9   C. Chen, *et al.*, Metal-free organic dyes derived from triphenylethylene for dye-sensitized solar cells: tuning of the performance by phenothiazine and carbazole, *J. Mater. Chem.*, 2012, **22.18**, 8994–9005.

10 A. Venkateswararao, K. R. Justin Thomas, C.-P. Lee, C.-T. Li and K.-C. Ho, Organic dyes containing carbazole as donor and π-linker: optical, electrochemical, and photovoltaic properties, *ACS Appl. Mater. Interfaces*, 2014, **6.4**, 2528–2539.

11 K. Narayanaswamy, T. Swetha, G. Kapil, S. S. Pandey, S. Hayase and S. Prakash Singh, Simple metal-free dyes derived from triphenylamine for DSSC: A comparative study of two different anchoring group, *Electrochim. Acta*, 2015, **169**, 256–263.

12 C. Sun, L. Yuanzuo, S. Peng and M. Fengcai, An experimental and theoretical investigation of the electronic structures and photoelectrical properties of ethyl red and carminic acid for DSSC application, *Materials*, 2016, **9.10**, 813.

13 G. Richhariya, A. Kumar, P. Tekasakul and B. Gupta, Natural dyes for dye sensitized solar cell: A review, *Renewable Sustainable Energy Rev.*, 2017, **69**, 705–718.

14 G. Calogero, I. Citro, C. Crupi and G. Di Marco, Absorption spectra and photovoltaic characterization of chlorophyllins as sensitizers for dye-sensitized solar cells, *Spectrochim. Acta, Part A*, 2014, **132**, 477–484.

15 M. Golshan, S. Osfouri, R. Azin and T. Jalali, Fabrication of optimized eco-friendly dye-sensitized solar cells by extracting pigments from low-cost native wild plants, *J. Photochem. Photobiol. A: Chem.*, 2020, **388**, 112191.

16 Chiang-Yu Chien and Ban-Dar Hsu, Optimization of the dye-sensitized solar cell with anthocyanin as photosensitizer, *Sol. Energy*, 2013, **98**, 203–211.

17 M. Hosseinnezhad, S. Rouhani and K. Gharanjig, Extraction and application of natural pigments for fabrication of green dye-sensitized solar cells, *Opto-Electron. Rev.*, 2018, **26.2**, 165–171.

18 T. Jalali, P. Arkian, M. Golshan, M. Jalali and S. Osfouri, Performance evaluation of natural native dyes as photosensitizer in dye-sensitized solar cells, *Opt. Mater.*, 2020, **110**, 110441.

19 M. Hamadanian, J. Safaei-Ghomi, M. Hosseinpour, R. Masoomi and V. Jabbari, Uses of new natural dye photosensitizers in fabrication of high potential dye-sensitized solar cells (DSSCs), *Mater. Sci. Semicond. Process.*, 2014, **27**, 733–739.

20 S. Suyitno, T. J. Saputra, A. Supriyanto and Z. Arifin, Stability and efficiency of dye - sensitized solar cells based on papaya-leaf dye, *Spectrochim. Acta, Part A*, 2015, **148**, 99–104.

21 A. Okello, B. O. Owuor, J. Namukobe, D. Okello and J. Mwabora, Influence of the pH of anthocyanins on the efficiency of dye sensitized solar cells, *Heliyon*, 2022, **8**(7), e099211-9.

22 M. N. Masood, Nabeel Mohammed, and Kameran Shukur Husien, Characterization of Eight Natural Dyes as Synthesizer for Dye-Sensitized Solar Cells Technology, 2023.

23 M. Golshan, S. Osfouri, A. Reza, T. Jalali and N. R. Moheimani, Co-sensitization of natural and low-cost dyes for efficient panchromatic light-harvesting using dye-sensitized solar cells, *J. Photochem. Photobiol., A*, 2021, **417**, 113345.

24 K. A. Kumar, K. Subalakshmi and J. Senthilselvan, *Co-sensitization of natural dyes for improved efficiency in dye-sensitized solar cell application*, AIP Publishing, 2016, vol. 1731, No. 1.

25 N. T. R. N. Kumara, P. Ekanayake, A. Lim, L. Y. C. Liew, M. Iskandar, L. C. Ming and G. K. R. Senadeera, Layered co-sensitization for enhancement of conversion efficiency of natural dye sensitized solar cells, *J. Alloys Compd.*, 2013, **581**, 186–191.

26 B. Alkali, J. B. Yerima, A. D. Ahmed and S. C. Ezike, Suppressed charge recombination aided co-sensitization in dye-sensitized solar cells-based natural plant extracts, *Optik*, 2022, **270**, 170072.

27 D. Spadaro, A. Tropea, I. Citro, S. Trocino, D. Giuffrida, F. Rigano and L. Mondello, Development of innovative dye sensitized solar cells (DSSCs) based on co-sensitization of natural microbial pigments, *Dyes Pigm.*, 2024, 112311.

28 P. Song, *et al.*, Insight into external electric field dependent photoinduced intermolecular charge transport in BHJ solar cell materials, *J. Mater. Chem. C*, 2015, **3.18**, 4810–4819.

29 U. Terranova and D. R. Bowler, Δ self-consistent field method for natural Anthocyanidin dyes, *J. Chem. Theory Comput.*, 2013, **9.7**, 3181–3188.

30 S. Namuangruk, *et al.*, Theoretical investigation of the charge-transfer properties in different meso-linked zinc porphyrins for highly efficient dye-sensitized solar cells, *Dalton Trans.*, 2014, **43.24**, 9166–9176.

31 R. Ranjitha, *et al.*, Structural and optical properties of Purpurin for dye-sensitized solar cells, *Spectrochim. Acta, Part A*, 2015, **149**, 997–1008.

32 P. Ren, Y. Zhang, Z. Luo, P. Song and Y. Li, Theoretical and experimental study on spectra, electronic structure and photoelectric properties of three nature dyes used for solar cells, *J. Mol. Liq.*, 2017, **247**, 193–206.

33 R. Sánchez-de-Armas, M. A. San Miguel, J. Oviedo and J. F. Sanz, Coumarin derivatives for dye sensitized solar

cells: a TD-DFT study, *Phys. Chem. Chem. Phys.*, 2012, **14**(1), 225–233.

34 F. Zanjanchi and J. Beheshtian, Natural pigments in dye-sensitized solar cell (DSSC): a DFT-TDDFT study, *J. Iran. Chem. Soc.*, 2019, **16**, 795–805.

35 Z. Xu, Y. Li, W. Zhang, S. Yuan, L. Hao, T. Xu and X. Lu, DFT/TD-DFT study of novel T shaped phenothiazine-based organic dyes for dye-sensitized solar cells applications, *Spectrochim. Acta, Part A*, 2019, **212**, 272–280.

36 I. C. Maurya, S. Singh, P. Srivastava, B. Maiti and L. Bahadur, Natural dye extract from Cassia fistula and its application in dye-sensitized solar cell: Experimental and density functional theory studies, *Opt. Mater.:X*, 2019, **90**, 273–280.

37 A. Ammasi, R. Iruthayaraj, A. P. Munusamy and M. Shkir, Enhancement of highly efficient flavone-based organic dyes with different anchoring groups effect in dye-sensitized solar cells using experimental and TD-DFT study, *J. Mater. Sci.: Mater. Electron*, 2023, **34.17**, 1331.

38 C. Qin and E. C. Aurora, DFT characterization of the optical and redox properties of natural pigments relevant to dye-sensitized solar cells, *Chem. Phys. Lett.*, 2007, **438.1–3**, 26–30.

39 O. Britel, A. Fitri, A. T. Benjelloun, A. Slimi, M. Benzakour and M. Mcharfi, Theoretical investigation of the influence of π-spacer on photovoltaic performances in carbazole-based dyes for dye sensitized solar cells applications, *J. Photochem. Photobiol., A*, 2022, **428**, 113870.

40 L. J. He, J. Chen, F. Q. Bai, R. Jia, J. Wang and H. X. Zhang, Fine-tuning π-spacer for high efficiency performance DSSC: a theoretical exploration with D–π–A based organic dye, *Dyes Pigm.*, 2017, **141**, 251–261.

41 A. M. Asaduzzaman and G. Schreckenbach, Computational studies on the interactions among redox couples, additives and TiO_2: implications for dye-sensitized solar cells, *Phys. Chem. Chem. Phys.*, 2010, **12**(43), 14609–14618.

42 Y. M. Hailu, M. T. Nguyen and J. C. Jiang, Theoretical study on the interaction of iodide electrolyte/organic dye with the TiO_2 surface in dye-sensitized solar cells, *Phys. Chem. Chem. Phys.*, 2020, **22**(45), 26410–26418.

43 M. Hussain, T. Jalali, L. Maftoon-Azad and S. Osfouri, Performance Evaluation of Natural Dye-Sensitized Solar Cells: A Comparison of Density Functional Theory and Experimental Data on Chlorophyll, anthocyanin, and Cocktail Dyes as Sensitizers, *ACS Appl. Electron. Mater.*, 2024, **6**(3), 1693–1709.

44 C. Lee, W. Yang and R. G. Parr, Development of the Colle-Salvetti correlation-energy formula into a functional of the electron density, *Phys. Rev. B*, 1988, **37.2**, 785.

45 W. J. Hehre, D. Robert and A. P. John, Self—consistent molecular orbital methods. XII. Further extensions of Gaussian—type basis sets for use in molecular orbital studies of organic molecules, *J. Chem. Phys.*, 1972, **56.5**, 2257–2261.

46 W. J. Hehre and W. A. Lathan, Self-consistent molecular orbital methods. XIV. Anextended Gaussian-type basis for molecular orbital studies of organic molecules. Inclusion of

second row elements, *J. Chem. Phys.*, 1972, **56**(11), 5255–5257.

47 W.-L. Ding, D.-M. Wang, Z.-Y. Geng, X.-L. Zhao and Y.-F. Yan, Molecular Engineering of Indoline-Based D–A–π–A Organic Sensitizers toward High Efficiency Performance from First-Principles Calculations, *J. Phys. Chem. C*, 2013, **117**(34), 17382–17398.

48 S. ElKhattabi, A. Fitri, A. T. Benjelloun, M. Benzakour, M. Mcharfi, M. Hamidi and M. Bouachrine, Theoretical investigation of electronic, optical and photovoltaic properties of alkylamine-based organic dyes as sensitizers for application in DSSCs, *transfer*, 2018, **3**, 7.

49 D. Fadili, S. M. Bouzzine and M. Hamidi, Study of the structural and optoelectronic properties of dye solar cells based on phosphonic acid anchoring by DFT functionals, *New J. Chem.*, 2021, **45**(5), 2723–2733.

50 T. Yanai, D. P. Tew and N. C. Handy, A new hybrid exchange–correlation functional using the Coulomb-attenuating method (CAM-B3LYP), *Chem. Phys. Lett.*, 2004, **393**(1–3), 51–57.

51 E. H. Rasheed and J. A.-A. Hadi, A theoretical enhancement of electronic transfer dynamics in the D35CPDT dye donor to TiO_2 acceptor. AIP Conference Proceedings. AIP Publishing, 2023, 2769. No. 1.

52 E. H. Rasheed and J. A.-A. Hadi, Theoretical insights into the study of the electronic transition reaction process from D35CPDT molecule dye to SnO_2 semiconductor. AIP Conference Proceedings, AIP Publishing, 2023, 2769, No. 1.

53 N. Wazzan and A. Irfan, Promising architectures modifying the D-π-A architecture of 2,3-dipentyldithieno[3,2-f:2′,3′-h]quinoxaline-based dye as efficient sensitizers in dye-sensitized solar cells: a DFT study, *Mater. Sci. Semicond. Process.*, 2020, **120**, 105260.

54 M. J. Frisch, G. W. Trucks, H. B. SCplegel, G. E. Scuseria, M. A. Robb, J. R. Cheeseman, G. Scalmani, V. Barone, G. A. Petersson and H. Nakatsuji, *et al.*, *Gaussian 16*, Gaussian Inc., Wallingford, CT, USA, 2016.

55 J. Zhang, H. B. Li, J. Z. Zhang, Y. Wu, Y. Geng, Q. Fu and Z. M. Su, A promising anchor group for efficient organic dye sensitized solar cells with iodine-free redox shuttles: a theoretical evaluation, *J. Mater. Chem. A*, 2013, **1**(44), 14000–14007.

56 N. Alsmani, S. A.-Q. Ohoud and W. Nuha, Performance enhancement of catechin graphene quantum dot nanocomposites functionalized with carboxyl and doped/decorated with boron towards dye-sensitized solar cell applications: DFT and TD-DFT calculations, *J. Mol. Graphics Modell.*, 2023, **121**, 108427.

57 L.-J. He, J. Chen, F.-Q. Bai, R. Jia, J. Wang and H.-X. Zhang, The influence of a dye–TiO_2 interface on DSSC performance: a theoretical exploration with a ruthenium dye, *RSC Adv.*, 2016, **6**, 81976–81982.

58 A. V. Vorontsov, Cluster models of photocatalytic anatase TiO_2 nanoparticles and their computational characterization, *Catal. Today*, 2015, **252**, 168–176.

59 S. Kohtani, A. Kawashima and H. Miyabe, Reactivity of trapped and accumulated electrons in titanium dioxide photocatalysis, *Catalysts*, 2017, **7**(10), 303.

60 T. Liu, J. Heimonen, Q. Zhang, C. Y. Yang, J. D. Huang, H. Y. Wu and S. Fabiano, Ground-state electron transfer in all-polymer donor: acceptor blends enables aqueous processing of water-insoluble conjugated polymers, *Nat. Commun.*, 2023, **14**(1), 8454.

61 W. M. Campbell, K. W. Jolley, P. Wagner, K. Wagner, P. J. Walsh, K. C. Gordon and D. L. Officer, Highly efficient porphyrin sensitizers for dye-sensitized solar cells, *J. Phys. Chem. C*, 2007, **111**(32), 11760–11762.

62 R. Ma, P. Guo, H. Cui, X. Zhang, M. K. Nazeeruddin and M. Grätzel, Substituent effect on the meso-substituted porphyrins: theoretical screening of sensitizer candidates for dye-sensitized solar cells, *J. Phys. Chem. A*, 2009, **113**(37), 10119–10124.

63 F. M. Mustafa, A. A. Abdel Khalek, A. A. Mahboob and M. K. Abdel-Latif, Designing Efficient Metal-Free Dye-Sensitized Solar Cells: A Detailed Computational Study, *Molecules*, 2023, **28**(17), 6177.

64 M. Xie, F. Q. Bai, J. Wang, C. P. Kong, J. Chen and H. X. Zhang, Theoretical description of dye regeneration on the TiO2–dye–electrolyte model, *Comput. Mater. Sci.*, 2016, **111**, 239–246.